Reprocessing of HIRS Satellite Measurements from 1980 to 2015: Development toward a Consistent Decadal Cloud Record

W. PAUL MENZEL, RICHARD A. FREY, EVA E. BORBAS, BRYAN A. BAUM, GEOFF CURETON, AND NICK BEARSON

Space Science and Engineering Center, University of Wisconsin–Madison, Madison, Wisconsin

(Manuscript received 28 March 2016, in final form 26 August 2016)

ABSTRACT

This paper presents the cloud-parameter data records derived from High Resolution Infrared Radiation Sounder (HIRS) measurements from 1980 through 2015 on the NOAA and MetOp polar-orbiting platforms. Over this time period, the HIRS sensor has been flown on 16 satellites from *TIROS-N* through *NOAA-19* and *MetOp-A* and *MetOp-B*, forming a 35-yr cloud data record. Intercalibration of the Infrared Advanced Sounding Interferometer (IASI) and HIRS on *MetOp-A* has created confidence in the onboard calibration of this HIRS as a reference for others. A recent effort to improve the understanding of IR-channel response functions of earlier HIRS sensor radiance measurements using simultaneous nadir overpasses has produced a more consistent sensor-to-sensor calibration record. Incorporation of a cloud mask from the higher-spatial-resolution Advanced Very High Resolution Radiometer (AVHRR) improves the subpixel cloud detection within the HIRS measurements. Cloud-top pressure and effective emissivity (εf, or cloud emissivity multiplied by cloud fraction) are derived using the 15-μm spectral bands in the carbon dioxide (CO_2) absorption band and implementing the CO_2-slicing technique; the approach is robust for high semitransparent clouds but weak for low clouds with little thermal contrast from clear-sky radiances. This paper documents the effort to incorporate the recalibration of the HIRS sensors, notes the improvements to the cloud algorithm, and presents the HIRS cloud data record from 1980 to 2015. The reprocessed HIRS cloud data record reports clouds in 76.5% of the observations, and 36.1% of the observations find high clouds.

1. Introduction

Cloud properties are derived from measurements from 1980 through 2015 made by the series of High Resolution Infrared Radiation Sounder (HIRS) sensors that have flown on 16 different polar-orbiting platforms. Over the course of this record, the HIRS sensors are generally available on both morning and afternoon platforms. Often there are multiple sensors in each orbit, especially in recent years; thus the complete HIRS record includes over 80 satellite years, or partial years, of data.

The HIRS record provides the only satellite-based infrared (IR) measurements from 1978 onward to the present in the 4.3- and 15-μm carbon dioxide (CO_2) absorption bands and in the 6.7-μm water vapor (H_2O) absorption band; both cloud and moisture properties can be studied with the same sensor. The cloud properties pertinent to this study are the cloud-top pressure (CTP), cloud-top temperature, cloud-top height, and cloud effective emissivity (εf, which is cloud emissivity ε multiplied by cloud fraction f). These parameters are derived using the 15-μm spectral bands in the CO_2-slicing approach, which has also been adopted for operational Moderate Resolution Imaging Spectroradiometer (MODIS) measurements (Menzel et al. 2008; Baum et al. 2012) from the National Aeronautics and Space Administration (NASA) *Terra* and *Aqua* platforms. The specific implementation used for this analysis is patterned after that of MODIS collection 6. The CO_2-slicing approach is effective for characterizing high-altitude, transmissive ice clouds and has been used in earlier studies with HIRS (Wylie and Menzel 1999; Wylie et al. 2005).

A series of operational HIRS sensors were flown on National Oceanic and Atmospheric Administration (NOAA) platforms beginning with *TIROS-N*, followed

Corresponding author address: W. Paul Menzel, Space Science and Engineering Center, University of Wisconsin–Madison, 1225 West Dayton St., Madison, WI 53706.
E-mail: paul.menzel@ssec.wisc.edu

DOI: 10.1175/JAMC-D-16-0129.1

TABLE 1. List of HIRS platforms, sensors, equator-crossing times, and periods of operation. The HIRS FOV size is nominally ~20 km at nadir for HIRS/2 and HIRS/3 sensors but decreased to 10-km resolution at nadir for HIRS/4. HIRS/3 has an improved signal-to-noise ratio over that from HIRS/2 sensors but the same FOV size. *TIROS-N* data were not available for this study.

Platform	Sensor	At-launch equator-crossing time (UTC)	Operational period
NOAA-6	HIRS/2	0800	27 Jun 1979–5 Mar 1983
NOAA-7	HIRS/2	1400	19 Aug 1983–24 Feb 1985
NOAA-8	HIRS/2	0700	20 Jun 1983–31 Oct 1985
NOAA-9	HIRS/2	1400	25 Feb 1985–7 Nov 1988
NOAA-10	HIRS/2	0730	17 Nov 1986–13 May 1991
NOAA-11	HIRS/2I	1400	8 Nov 1988–10 Apr 1995
NOAA-12	HIRS/2	0730	14 May 1991–30 May 1997
NOAA-14	HIRS/2I	1400	11 Apr 1995–19 Mar 2001
NOAA-15	HIRS/3	0730	15 Dec 1998–15 Oct 2002
NOAA-16	HIRS/3	1400	20 Mar 2001–29 Aug 2005
NOAA-17	HIRS/3	1000	16 Oct 2002–1 Jun 2009
NOAA-18	HIRS/4	1400	30 Aug 2005–1 Jun 2009
NOAA-19	HIRS/4	1400	2 Jun 2009–present
MetOp-A	HIRS/4	1000	21 May 2007–23 Apr 2013
MetOp-B	HIRS/4	1000	24 Apr 2013–present

by *NOAA-6* through *NOAA-19*. HIRS is also recently found on the *MetOp-A* and *MetOp-B* platforms operated by the European Organisation for the Exploitation of Meteorological Satellites (EUMETSAT). A companion sensor on each of these platforms is the Advanced Very High Resolution Radiometer (AVHRR). Concurrent with efforts to infer cloud properties from HIRS, a separate task is ongoing to provide cloud properties from the AVHRR record (Heidinger et al. 2014). An AVHRR imager is present on each of the platforms that carry a HIRS. The Clouds from AVHRR—Extended (CLAVR-x) project provides cloud products at Global Area Coverage (GAC) 4-km resolution. The cloud climate component of CLAVR-x is called AVHRR Pathfinder Atmospheres—Extended (PATMOS-x; Foster and Heidinger 2013).

The HIRS platforms, years of their operational coverage, and total years of service are provided in Table 1 (*TIROS-N* data were not available for this study; hence our cloud data record starts in 1980). ''Operational coverage'' refers to the period for which measurements from a specific HIRS were used to derive operational products, which is generally only a portion of the total working life of the sensor. Unlike the NASA Earth Observing System *Terra* and *Aqua* satellites, which have fixed equator-crossing times over the entire life of the missions, the NOAA platforms had relatively stable equatorial overpass times during the operational portion of their tenure, after which the orbits were often allowed to decay over time.

To properly interpret the extended HIRS record, one has to understand the calibration characteristics of each sensor, the spectral response functions (SRF) of each channel for each sensor, and the impact of orbital drift on the inferred cloud properties. Since the study presented in Wylie et al. (2005), a variety of changes have been made to the processing chain and are summarized below. Where possible, reference is made to other studies that provide greater detail. Further description, where warranted, is provided in section 2.

A summary of algorithm and calibration refinements employed in the current study is as follows:

1) Through an extensive recalibration process (Cao and Goldberg 2009; Chen and Cao 2012; Chen et al. 2013), the HIRS measurements have become more consistent from platform to platform (via radiative transfer calculations performed in the CO_2 spectral bands). The process for improving the calibration involves using the high-spectral-resolution IR sensor Infrared Advanced Sounding Interferometer (IASI) to investigate the SRFs for CO_2 and H_2O bands. The calibration is stepped back in time using simultaneous nadir overpasses (SNOs). In the absence of SNOs, the geosounder data from the CO_2 spectral bands [from the Visible-Infrared Spin-Scan Radiometer (VISSR) Atmospheric Sounder (VAS)] were used in a double-differencing approach to connect *NOAA-6* onward with *NOAA-9*. Shi et al. (2008) noted scene-dependent HIRS intersatellite biases that the HIRS recalibration process mitigates.
2) In Wylie et al. (2005), the determination of whether a HIRS field of view (FOV) was clear sky or cloudy was based on multiple passes through the data and was a source of uncertainty given the large FOV and the difficulty in discerning low-level clouds. In this study, the PATMOS-x cloud mask and cloud type (Heidinger et al. 2014) within each HIRS FOV

TABLE 2. List of HIRS channels. For HIRS/2I, channel 10 changed from 1225 to 802 cm^{-1} (from 8.2 to 12.5 μm).

Channel	Central wavenumber (cm^{-1})			Principal absorbing components	Peak in weighting function (hPa)
	HIRS/2/2I	HIRS/3	HIRS/4		
1	668	669	669	CO_2	25
2	680	680	680	CO_2	50
3	691	690	690	CO_2	70
4	703	703	703	CO_2	250
5	717	716	716	CO_2	400
6	733	733	733	CO_2	600
7	749	749	749	CO_2	900
8	899	900	900	Window	Surface
9	1032	1030	1030	O_3	30
10	1225	802	802	H_2O	Surface
11	1365	1365	1365	H_2O	500
12	1483	1533	1533	H_2O	300
13	2190	2188	2188	N_2O	1000
14	2209	2210	2210	N_2O	600
15	2243	2235	2235	CO_2/N_2O	700
16	2276	2245	2245	CO_2/N_2O	400
17	2359	2420	2420	CO_2	Surface
18	2518	2515	2515	Window	Surface
19	2668	2660	2660	Window	Surface
20	14 549	14 500	14 500	Visible	Cloud/albedo

determine the cloud fraction and phase. The AVHRR products are collocated within the HIRS FOV using the method of Nagle and Holz (2009).

3) The IR channels used are affected primarily by CO_2, O_3, and H_2O. For radiative calculations, the CO_2 concentration is increased over the 40-yr time period following a sinusoidal approximation, H_2O concentrations are provided by the National Centers for Environmental Prediction (NCEP) Climate Forecast System Reanalysis (CFSR; Saha et al. 2010) product at 0.5° resolution, and O_3 profiles are estimated from a combination of CFSR and climatological values.
4) The algorithm used for the MODIS collection-6 cloud-top pressure/height operational products (Menzel et al. 2008; Baum et al. 2012) is adopted here. This includes detection of deep tropical convective clouds that potentially overshoot the tropopause [upper-tropospheric/lower-stratospheric (UTLS) clouds] as introduced in Schmetz et al. (1997). Kolat et al. (2013) have described the UTLS cloud-detection algorithm applied to HIRS data.

Section 2 describes the sensors, data products, and radiative transfer model used in this study. Section 3 briefly describes the algorithm refinements, with details provided in earlier studies. Section 4 presents the HIRS cloud record over the period from 1980 through 2015. Section 5 offers conclusions and comments on continuation of the HIRS cloud dataset beyond the lifetime of the HIRS instruments. Regional studies and inferences about decadal changes remain the focus of future work.

2. Data and models

a. HIRS

The HIRS sensor has remained basically unchanged over the course of more than 30 years, taking measurements at 19 IR channels (see Table 2) and one solar channel. This is a sounding instrument that takes measurements using a "stop and stare" approach in which a rotating filter wheel steps through the various IR-channel measurements. For the HIRS sensors, a scan takes 6.4 s and provides the radiance measurements for 56 FOVs over a swath of approximately 2160 km. With HIRS/4 the FOV was improved from the earlier contiguous 20 km to a sampled 10 km. An SRF is determined before launch for each HIRS IR channel on every sensor, but recent comparisons between MODIS and Atmospheric Infrared Sounder (AIRS) indicate that slight adjustments to the IR-channel SRFs may be necessary to achieve greater radiometric consistency (e.g., Tobin et al. 2006; Baum et al. 2012). The same issue is found to be true for the HIRS sensors. Comprehensive global and seasonal comparison of the radiances measured by the broadband HIRS and the high-spectral-resolution IASI on *MetOp-A* has suggested spectral shifts for the *MetOp-A* HIRS and established it as a reference sensor. Intercalibration of the *MetOp-A* HIRS with earlier HIRS using SNOs has helped to create a more consistent sensor-to-sensor calibration record (see Table 3). Studies by Cao and Goldberg (2009) and Chen et al. (2013) provide an extensive

TABLE 3. Suggested spectral shifts (in wavenumber) suggested by IASI and simultaneous nadir overpasses; positive values indicate a shift to larger wavenumber [from Chen et al. (2013)]. No SRF shifts were found to be necessary for channel 6 (13.7 μm), and no shifts were applied to *NOAA-8*.

Platform	Channel 4 (14.2 μm)	Channel 5 (14.2 μm)	Channel 7 (14.2 μm)
NOAA-6	0.31	0.70	0.70
NOAA-7	−0.18	0.10	1.20
NOAA-9	0.43	2.66	−0.48
NOAA-10	0.95	1.56	−0.93
NOAA-11	1.72	2.05	0.15
NOAA-12	0.47	2.23	−2.06
NOAA-14	1.97	3.13	1.22
NOAA-15	−0.21	0.27	1.01
NOAA-16	0.22	0.62	0.47
NOAA-17	0.54	0.72	0.44
NOAA-18	−0.71	−0.37	−0.49
NOAA-19	None	−0.12	0.10
MetOp-A	−0.15	0.10	−0.15
MetOp-B	−1.21	−0.43	−0.54

reevaluation of the HIRS calibration and SRF characteristics that are adopted in this study.

b. *Clouds from PATMOS-x*

The resolution of the AVHRR GAC data is 4 km (constructed from 4 of every 5 pixels on every third AVHRR scan line at native 1-km resolution), whereas the resolution of the HIRS/2 and HIRS/3 FOV is 20 km, and that of HIRS/4 is 10 km. We note earlier efforts to collocate AVHRR and HIRS (e.g., Aoki 1985; Baum et al. 1992; Frey et al. 1996). The HIRS–AVHRR collocation is performed for the sensor pair on each platform using the approach discussed in Nagle and Holz (2009). The number of collocated AVHRR pixels found within HIRS/2 and HIRS/3 FOVs ranges between 20 (nadir) and 35 (edge of scan), and it ranges between 5 and 12 for HIRS/4.

For the operational days attributed to HIRS, the AVHRR data collocated with the HIRS data are missing for 7.2% of the HIRS data record; this increases to 12.7% when considering the PATMOS-x cloud mask because of data-quality issues. The problems were most prevalent for *NOAA-6*.

Determination of whether a HIRS FOV is clear or cloudy is accomplished by consulting the higher-spatial-resolution AVHRR PATMOS-x cloud mask. The cloud probability for any given AVHRR pixel is provided from a naïve Bayesian cloud-detection algorithm (Heidinger et al. 2012). If an AVHRR pixel has a cloud probability that is greater than 0.5, it is labeled as cloudy. For a HIRS FOV to be labeled as cloudy, at least 15% of the collocated AVHRR pixels must have a cloud probability of greater than 0.5.

The CLAVR-x products also include a land–sea tag as well as a cloud-phase designation (Pavolonis et al. 2005). The latter is used to screen CO_2-slicing retrievals. Over water, if the fraction of water-phase clouds within the HIRS FOV is greater than or equal to 0.75 and the HIRS CTP is greater than or equal to 440 hPa, then the CTP is based solely on the infrared-window 11-μm channel (HIRS channel 8). From the MODIS experience

TABLE 4. Summary of HIRS reprocessing of cloud properties.

Spectral bands used: IR only using IR CO_2- and IR-window bands
Orbits processed: Both ascending and descending for a.m. and p.m. local crossings
Coverage: Contiguous FOVS (with 20-km resolution at nadir) for HIRS/2/2I/3 over entire globe within 32° of nadir; for HIRS/4 this changed to 10-km FOVS sampled every 20 km
Cloud mask: PATMOS-x cloud mask applied to AVHRR GAC data plus CO_2-channel screening of thin cirrus
Clear radiance estimate: Explicit forward radiance calculation (from NCEP CFSR) with calculated minus measured radiance bias adjustment
Cloud parameters processed: Effective cloud amount and cloud-top pressure
Cloud classification: High (CTP < 440 hPa), middle (440 ≤ CTP ≤ 680 hPa), and low (CTP > 680 hPa) along with thin ($\varepsilon f < 0.5$), thick ($0.5 \le \varepsilon f \le 0.95$), and opaque ($\varepsilon f > 0.95$)
Diurnal segmentation: By LT and θ_0 as follows: Nighttime ($\theta_0 > 85°$ and 0000 ≤ LT < 1200), morning ($\theta_0 \le 85°$ and 0000 < LT < 1200), afternoon ($\theta_0 \le 85°$ and 1200 ≤ LT < 2400), and evening ($\theta_0 > 85°$ and 1200 < LT < 2400)
Strength: Good detection of high thin clouds even in partly cloudy FOVs
Weakness: Thermal contrast for low clouds and polar clouds is often too small for reliable cloud detection and cloud-property evaluation

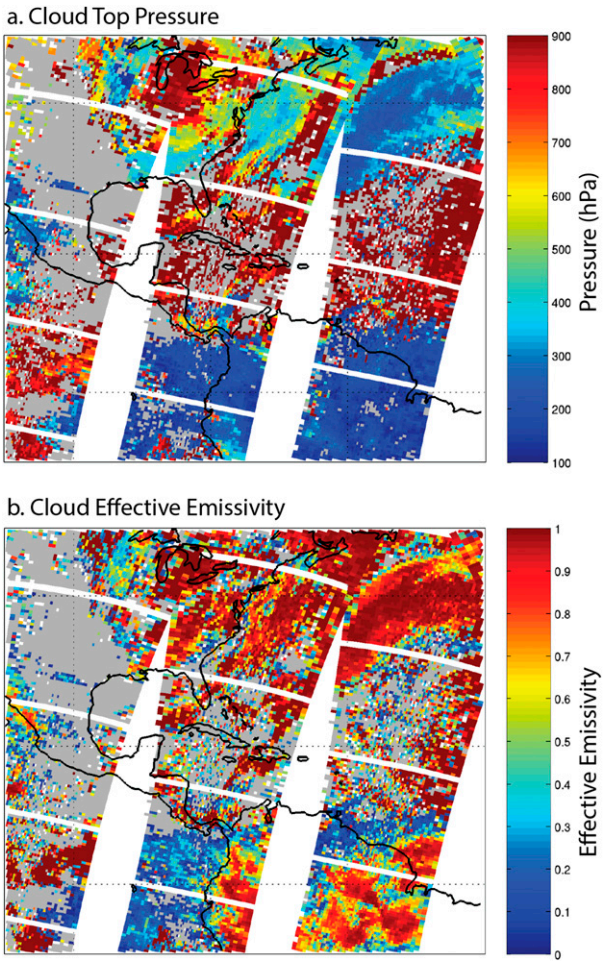

FIG. 1. (a) CTP (hPa) determined from radiances measured by the HIRS on *MetOp-A* on 19 Jan 2009. High clouds (CTP < 440 hPa) were found in 36% of these FOVS, midlevel clouds (440 ≤ CTP ≤ 680 hPa) were found in 8%, and low clouds (CTP > 680 hPa) were found in 24%. Clear skies (the gray color) were found in the remaining 32%. (b) Associated cloud effective emissivities (cloud fraction times cloud emissivity), for which opaque clouds ($\varepsilon f > 0.95$) were found in 17% of these FOVS, thick clouds ($0.5 \le \varepsilon f \le 0.95$) were found in 23%, and thin clouds ($\varepsilon f < 0.5$) were found in 28%. The calibration gaps appear every 40 scan lines when HIRS views space and the internal blackbodies. Data gaps among the 56 FOV swaths are also evident.

(Baum et al. 2012), better CTPs have been realized for water clouds when assuming an opaque cloud requiring only a cloud-fraction adjustment (available here from the AVHRR-based cloud mask).

c. *Radiative transfer model and CFSR meteorological product*

An issue of paramount importance for the inference of cloud properties is the determination of the clear-sky radiance within a HIRS FOV. The PATMOS-x cloud mask provides one of the largest improvements in the detection of clear-sky pixels within a HIRS FOV. In addition, screening for thin cirrus is applied to the PATMOS-x-derived clear-sky HIRS FOVs using the CO_2 channels (this additional CO_2-slicing screening finds thin cirrus in 1.7% of the HIRS observations that was missed by the AVHRR cloud mask). Along with the measured clear-sky radiance for each of the HIRS channels, a radiative transfer calculation is also performed using the Pressure Layer Fast Algorithm for Atmospheric Transmittances (PFAAST) model (Hannon et al. 1996). The PFAAST radiative transfer calculations are performed at 101 vertical levels using atmospheric profiles of temperature, humidity, and ozone (O_3) that are based on the CFSR data at 0.5° spatial resolution.

The clear-sky measurements in the HIRS CO_2 absorption bands are compared with forward-model calculations of clear-sky channel radiances using the NCEP CFSR temperature, moisture, and ozone soundings. The comparison of the measured-to-modeled clear-sky radiances is made to establish the clear-sky radiance biases; there are always differences between measured and calculated clear-sky radiances. Biases are determined daily and composited into monthly clear-sky radiance biases (CSRBs); this radiance bias is used retrospectively for the whole month.

Improvements in clear-sky radiance calculations were made by 1) implementing a 101-level radiative transfer model, PFAAST (Hannon et al. 1996; Strow et al. 2006), in the data reduction, 2) adjusting the ozone profile between 10 and 100 hPa to values from the NCEP–NCAR reanalysis (Kalnay et al. 1996) (so that CO_2 radiances influenced by O_3 profiles are calculated more accurately), and 3) using a sinusoidally varying CO_2 concentration that increases 1.5 ppmv yr^{-1} from 337.5 in January of 1980 with a seasonal amplitude change of ±3 ppmv. Thus,

$$CO_2(x) = [mx + a\sin(2\pi x)/365] + b, \qquad (1)$$

where $m = 1.5$ ppmv/365, $b = 337.5$ ppmv, $a = 3$ ppmv, and $x =$ number of days since 1 January 1980.

CSRBs are maintained for HIRS bands 4–7 on both daily and monthly scales as part of the cloud-properties processing chain. Monthly mean 1° zonal biases are used to correct individual forward-model calculations in the CO_2-slicing algorithm to account for uncertainties in the input CFSR-profile data.

3. Method

The implementation of the CTP algorithm (level-2 processing of individual HIRS FOVs) for the HIRS data

TABLE 5. Mean and rms of the daily frequency of occurrence for each cloud category for 1980–2015 determined from the near-nadir HIRS observations (view angle $< 32°$) between 60°S and 60°N. Clouds are categorized by thin, thick, and opaque as well as low-, mid-, and high-level clouds; 23.5% represented clear skies. The values from Table 2a of Wylie et al. (2005) for 1979–2001 are indicated in italics. Note that low thin and thick clouds are most likely clouds that partially fill the HIRS FOV.

	Thin ($\varepsilon f < 0.5$)	Thick	Opaque ($\varepsilon f > 0.95$)	Total
High (CTP $<$ 440 hPa)	20.1 ± 2.1 (*15*)	14.0 ± 1.8 (*15*)	2.0 ± 1.2 (*3*)	36.1 (*33*)
Middle	4.5 ± 0.8 (*5*)	4.8 ± 0.9 (*7*)	1.8 ± 1.0 (*6*)	11.1 (*18*)
Low (CTP $>$ 660 hPa)	7.7 ± 1.2 (*0*)	8.7 ± 1.6 (*1*)	12.9 ± 2.7 (*23*)	29.3 (*24*)
Total	32.3 (*20*)	27.5 (*23*)	16.7 (*32*)	76.5 (*75*)

record is analogous to that of the 5-km collection-6 MODIS (MOD06) in most ways. For example, use of collocated AVHRR GAC pixels within HIRS FOVs is analogous to use of MODIS 1-km pixels within 5 × 5 pixel regions for MODIS CTP retrievals; both algorithms use the 15% cloud-coverage threshold for generating retrievals. Use of CFSR-model atmospheric-profile data is similar to the use of NCEP Global Data Assimilation System data for MODIS. MODIS also uses the PFAAST forward model for simulation of MODIS clear-sky radiances from ancillary profile data. The biggest difference between the HIRS and MODIS algorithms is the aggregation time of the zonal-mean clear-sky radiances used for bias correction in radiative transfer calculations; because of the larger FOV size and correspondingly fewer clear-sky observations, the HIRS process uses monthly-mean data, whereas the MODIS process uses 8-day means.

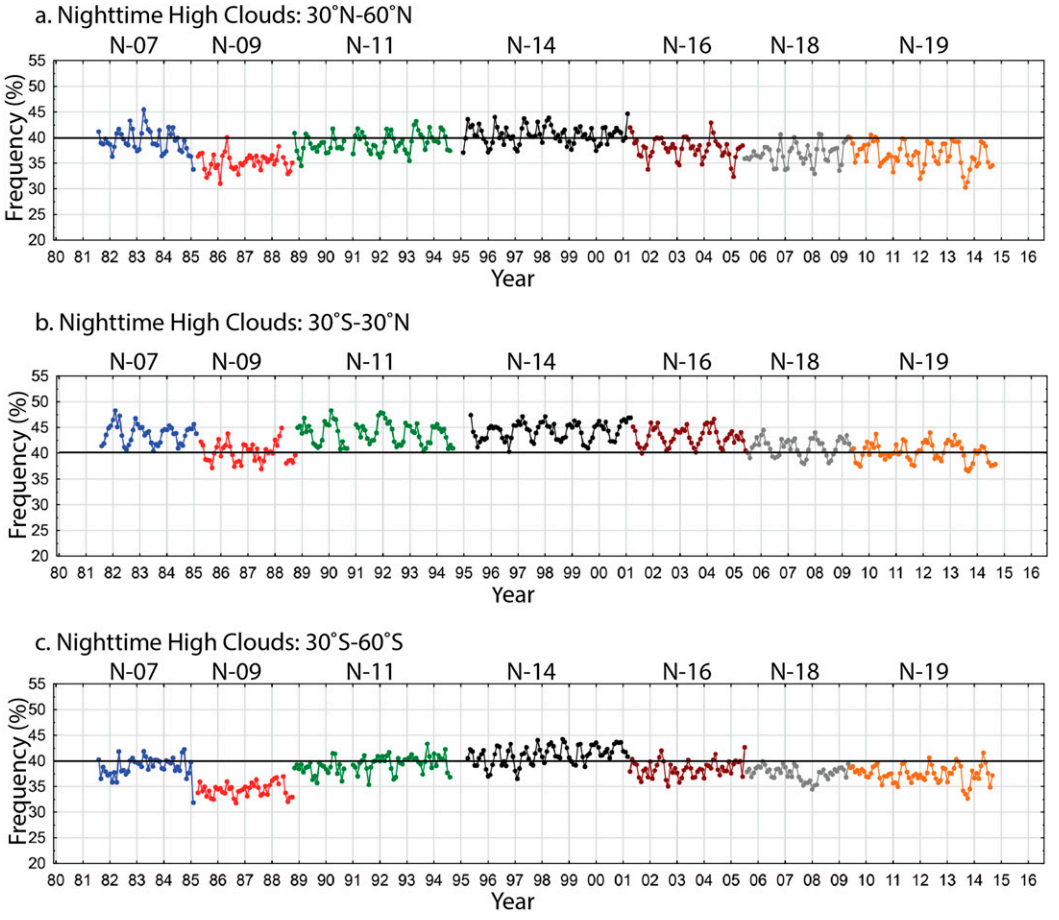

FIG. 2. For HIRS, the percentage of nighttime observations from 1981 through 2014 that contained high clouds for (a) 30°–60°N, (b) 30°S–30°N, and (c) 30°–60°S and the percentage of evening observations from 1980 through 2015 that contained high clouds for (d) 30°–60°N, (e) 30°S–30°N, and (f) 30°–60°S.

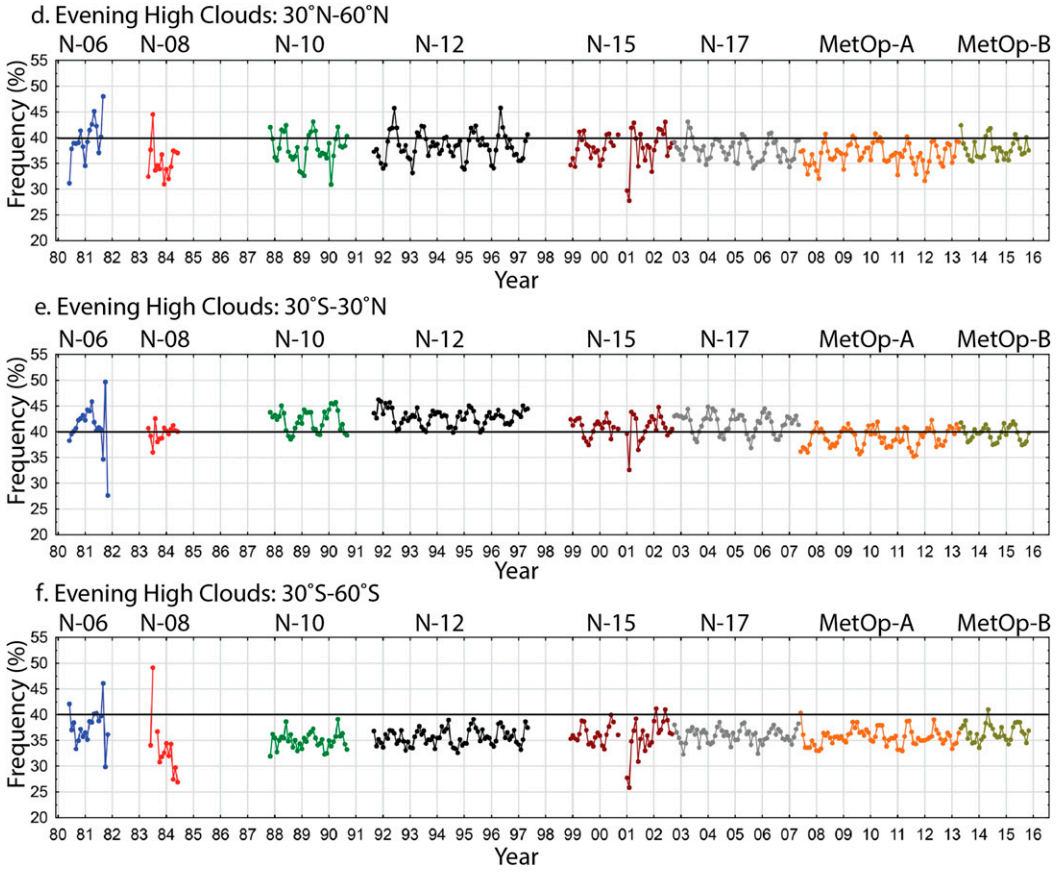

FIG. 2. (*Continued*)

Last, the cloud-detection threshold (clear minus cloudy radiance values that must be exceeded for the CO_2-slicing bands to be engaged in the cloud algorithm) was reduced from 1.0 mW m^{-2} sr^{-1} cm used in Wylie et al. (2005); in this work 0.5 mW m^{-2} sr^{-1} cm is used. This was suggested by prelaunch measured noise of less than 0.1 mW m^{-2} sr^{-1} cm in the CO_2 spectral bands. In cases for which these thresholds are not met, the default infrared-window determination of (assumed) opaque CTP is reported. With the smaller cloud-detection threshold, more high and optically thin clouds (that were misclassified as low clouds by the IR window in about 5% of the HIRS observations) are now properly retrieved via CO_2 slicing. This increased detection occurs mostly around high-cloud edges (Kolat 2010).

4. Cloud results for 35+ years of HIRS data

A set of filtering conditions is established and adopted in a space–time gridding approach (Smith et al. 2013) assuming an equal-angle grid at 0.5° resolution for all products. The filtering conditions include a limitation on viewing zenith angle (only data within 32° from nadir are used), definition of low-, mid-, and high-level clouds by CTP thresholds, classification by effective cloud emissivity, and finally separation of cloud properties into four time periods of night, morning, afternoon, and evening. Clouds are stratified as high (CTP $<$ 440 hPa), middle (440 $\leq$ CTP $\leq$ 680 hPa), and low (CTP $>$ 680 hPa). The clouds are also classified by effective cloud emissivity, as thin ($\varepsilon f < 0.5$), thick ($0.5 \leq \varepsilon f \leq 0.95$), and opaque ($\varepsilon f > 0.95$), where the cloud fraction f is determined directly from the collocated AVHRR cloud mask. Because the sensor orbit drifts over time, the cloud-properties retrievals are divided according to the local time (LT) and the solar zenith angle θ_0 as follows. "Nighttime" is defined as $\theta_0 > 85°$ and $0000 \leq$ LT < 1200, "morning" is defined when $\theta_0 \leq 85°$ and $0000 <$ LT < 1200, "afternoon" is defined when $\theta_0 \leq 85°$ and $1200 \leq$ LT < 2400, and "evening" is defined when $\theta_0 > 85°$ and $1200 <$ LT < 2400. Operational morning and evening observations were taken by *NOAA-6*, *NOAA-8*, *NOAA-10*, *NOAA-12*, *NOAA-15*, *NOAA-17*, *MetOp-A*, and *MetOp-B*. Operational afternoon and nighttime observations came from *NOAA-7*, *NOAA-9*,

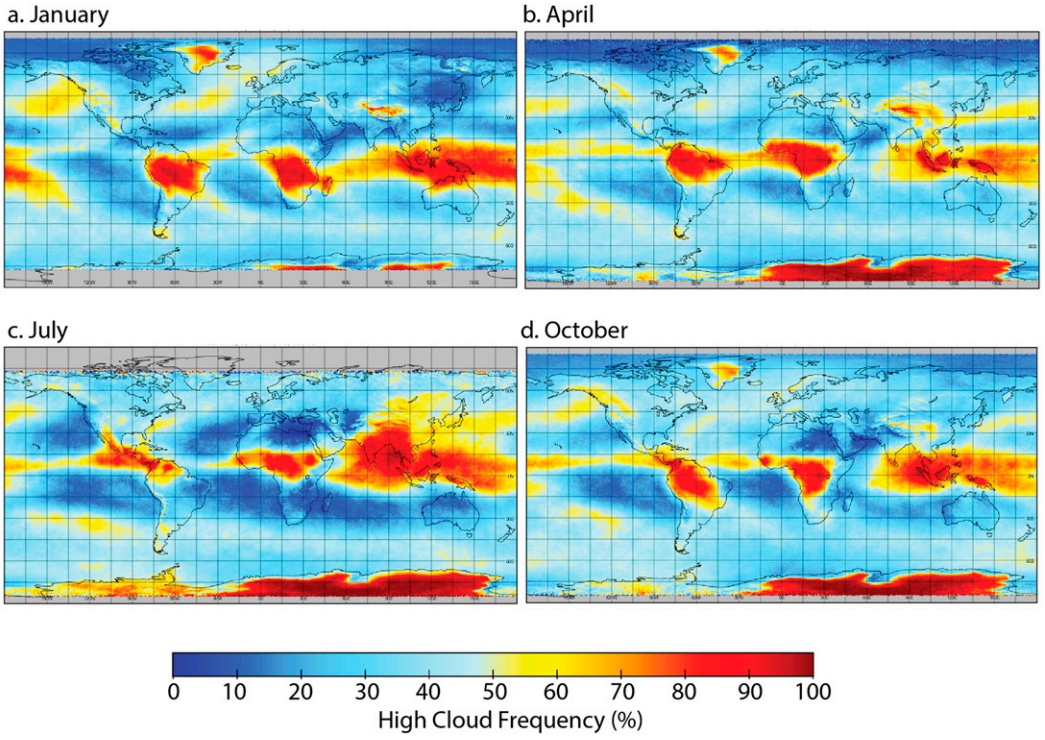

FIG. 3. The 1980–2015 mean HIRS high-cloud detection at night for (a) January, (b) April, (c) July, and (d) October. Heidinger et al. (2016) note that AVHRR detects 5%–10% too few clouds over the Tibetan Plateau and the Andes and 15% too many clouds over Antarctica and Greenland; these are regions where the absence of a water vapor channel on AVHRR makes a significant difference.

NOAA-11, *NOAA-14*, *NOAA-16*, *NOAA-18*, and *NOAA-19*. During their extended nonoperational lifetimes, some of the NOAA sensors drifted out of their designated diurnal sampling times; we confine this data analysis to the operational time periods so that orbital drift is less than 2 h (except for *NOAA-11*, *NOAA-12*, and *NOAA-14*, where it is less than 4 h).

Cloud observations from *NOAA-6* onward were processed from 60°N to 60°S, including both ascending and descending orbits. Table 4 summarizes the HIRS cloud processing that is presented in the following sections. The reprocessed HIRS (with spectral shift applied) cloud trends obtained from the operational days on NOAA and MetOp (see Table 1) are now presented.

a. Some example swaths of HIRS CTP and εf

An example of the HIRS CTP and cloud εf fields derived for several swaths on 19 January 2009 is shown in Fig. 1. In these granules HIRS finds a variety of clouds and clear skies (shown in gray). Thick opaque high clouds over eastern South America taper off to thinner high clouds going toward the cloud edges. It is important to note that CTP does not vary with εf, as would be expected when the semitransparency correction is done properly. A winter storm is evident over the eastern half of the United States and adjacent Atlantic Ocean. High clouds are associated with a double-barreled low pressure system, one centered over Nova Scotia and the other over the southeastern United States. In the northern Atlantic Ocean, a bank of high opaque clouds sits north of scattered low clouds; the CTPs for the latter are derived from the IRW, and the cloud fraction comes directly from the subpixel cloud characterization derived from PATMOS-x.

b. Average cloud detection for the HIRS data record

Table 5 shows the mean and rms of the daily frequency of occurrence for each cloud category for 1980–2015 determined from the HIRS observations between 60°S and 60°N. Clouds are categorized by thin, thick, and opaque as well as low-, mid-, and high-level clouds; 23.5% of the HIRS observations were declared to be free of clouds, and 76.5% had clouds present. CO_2 slicing determined the CTPs for 36.1% of all observations to be less than 440 hPa. The IR window determined 29.3% of all observations to be low clouds with CTP greater than 660 hPa. Thin clouds

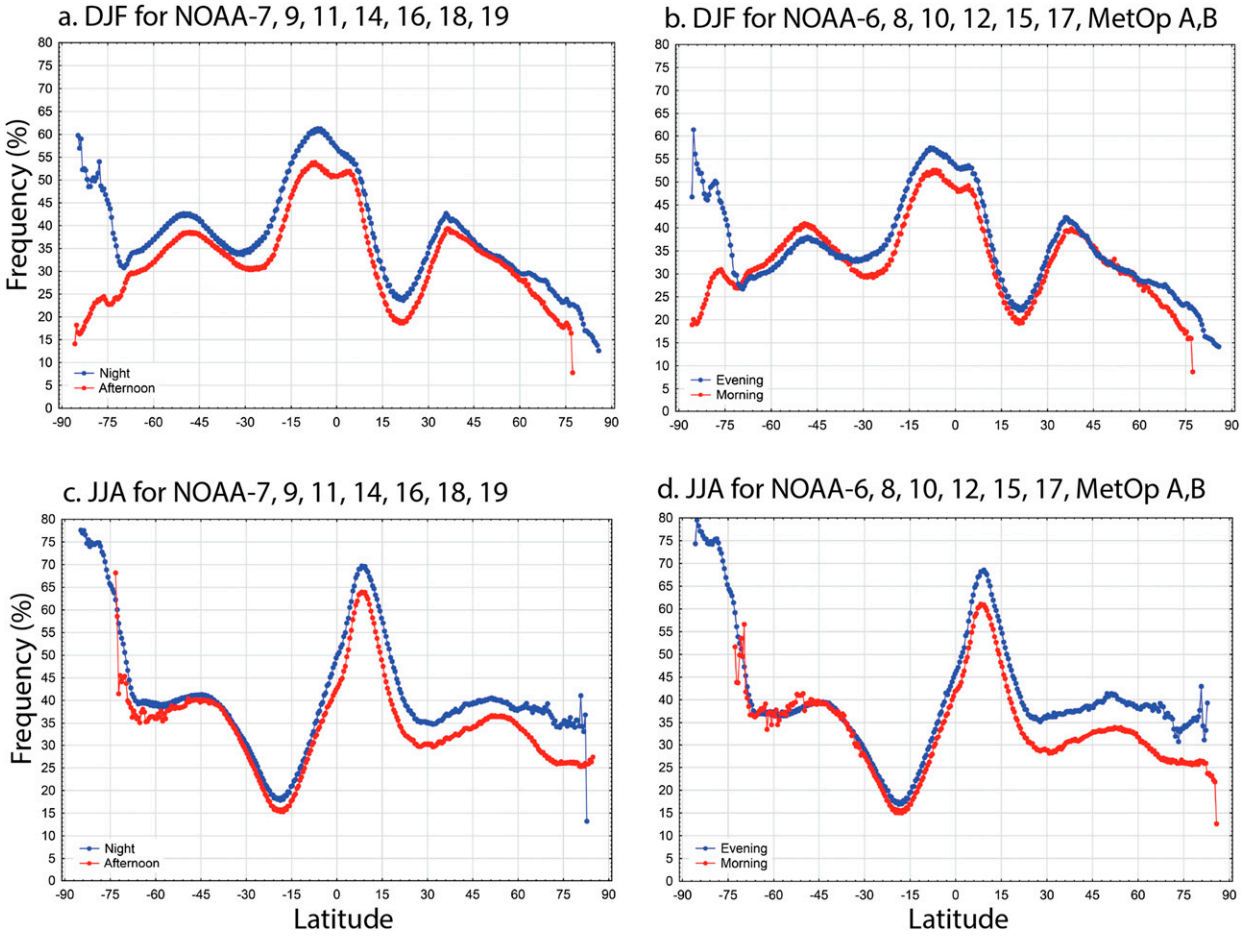

FIG. 4. Latitudinal average of the night, morning, evening, and afternoon high-cloud detection for (a),(b) DJF and (c),(d) JJA from 1980 to 2015.

($\varepsilon f < 0.5$) were found in 32.3% of all of the HIRS observations, and thick clouds ($\varepsilon f \geq 0.5$ and ≤ 0.95) were found in 27.5% of observations. Opaque clouds completely filling the HIRS FOV were found in 16.7% of all of the HIRS observations. The rms scatter about the mean values for each cloud group ranges from 0.8% to 2.7%; the large values are indicative of the sensor-to-sensor differences that were mitigated but not eliminated by the recalibration efforts. When a record for one year from a single sensor (not shown) is evaluated, the mean values remain similar but the rms scatter values now range from 0.3% to 1.1%; the single-sensor distribution of HIRS cloud observations does not vary appreciably from day to day or from season to season.

These results are in general agreement with those found in Wylie et al. (2005). Both report roughly the same cloud detection in the HIRS observations (76.5% in this study rather than the earlier 75%). Both find the same high-cloud occurrence (36.1% as compared with the earlier 33%). This study finds fewer midlevel clouds (11.1% rather than 18%), however; this result can be attributed to the top-down approach used here in which the most opaque channel pair that sees the cloud determines the CTP (see Menzel et al. 2008) rather than using all of the channel pairs to determine a mean CTP [as was used in Wylie et al. (2005)]. In addition, the frequency of low opaque clouds has decreased (12.9% rather than 23%) for two reasons. First, with the AVHRR characterization of the HIRS FOV cloud fraction, this study finds more thin and thick low clouds (16.4% in this study rather than 1%) that were previously classified as opaque. Second, the reduced cloud-detection threshold used here enables the determination of more high thin clouds at the expense of low opaque clouds. Overall in this study, CO_2 slicing is used more selectively (only in ice clouds and not in water clouds) and the HIRS FOV cloud-fraction characterizations reduce opaque cloud designations. The remainder of this paper will focus on the HIRS high-cloud

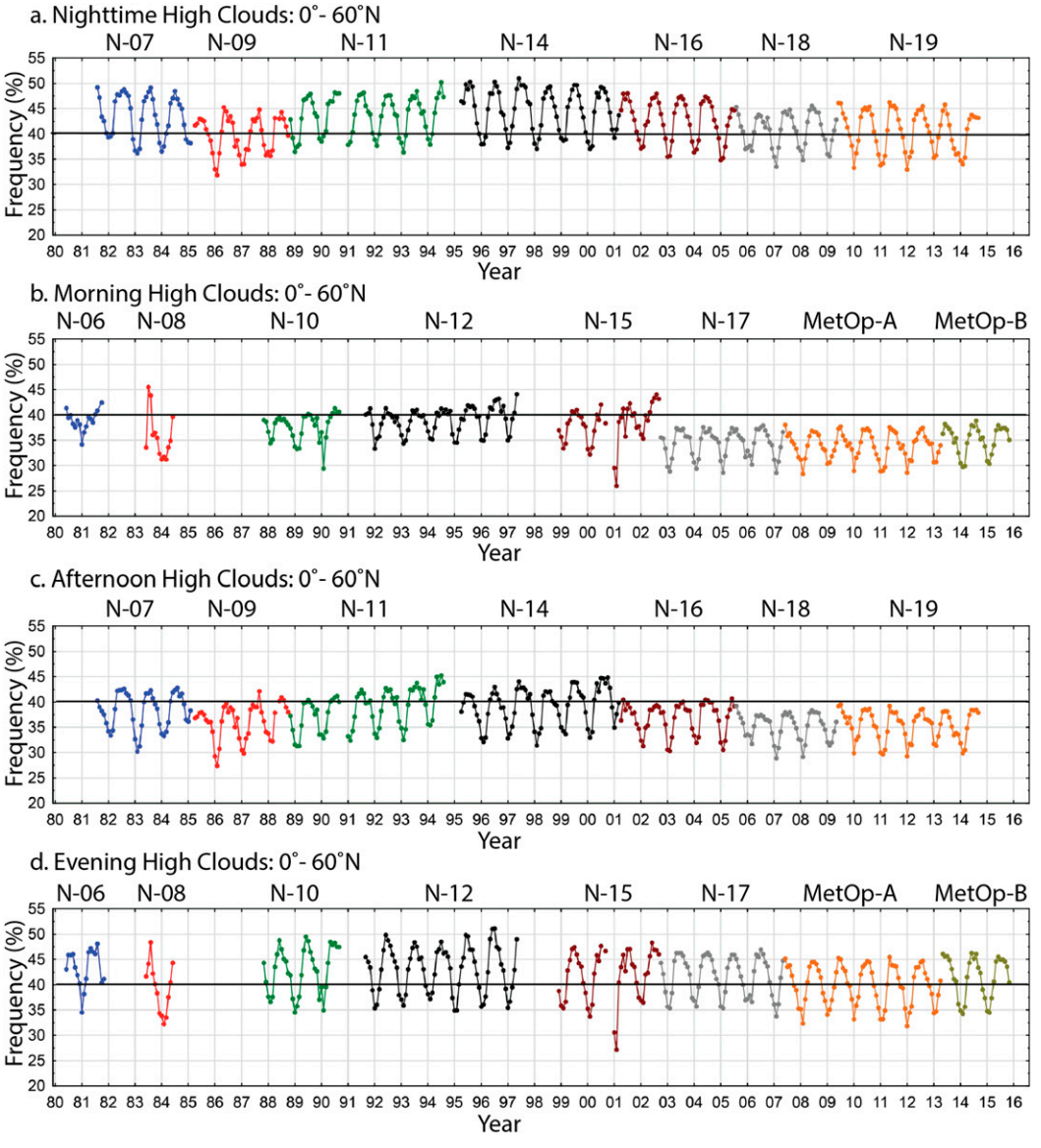

FIG. 5. Percentage of HIRS observations that contained high clouds in the (a)–(d) Northern Hemisphere (0°–60°N) and the (e)–(h) Southern Hemisphere (0°–60°S) from 1980 to 2015.

results, for which the CO_2-slicing algorithm plays the major role.

c. *Monthly high-cloud results for the midlatitudes and tropics*

Figures 2a–c show the monthly progression of the percentage of HIRS observations at night from *NOAA-7* to *NOAA-19* in which a high cloud (CTP $<$ 440 hPa) is detected (this relies primarily on spectral bands 4 and 5 at 14.2 and 14.0 μm, respectively). High clouds in the upper troposphere (above 6 km) are found in ~35%–40% of the HIRS midlatitude observations; this percentage increases to between 40% and 45% of the tropical observations. The seasonal change in high-cloud detection goes from a December–February (DJF) maximum to a June–August (JJA) minimum, dropping ~6%. Sensor-to-sensor differences are still evident, especially with *NOAA-9* and *NOAA-14*. A surprising feature of all of these data is that the global (excluding polar regions) high-cloud cover has shown little change despite dramatic volcanic and El Niño events over the time span of this study.

Figures 2d–f present the frequency of high-cloud detection in the evening for the satellites from *NOAA-6* to *MetOp-B*. Despite the significant gaps in the HIRS coverage in the early years and obvious deviations in the data quality, the general consistency of evening

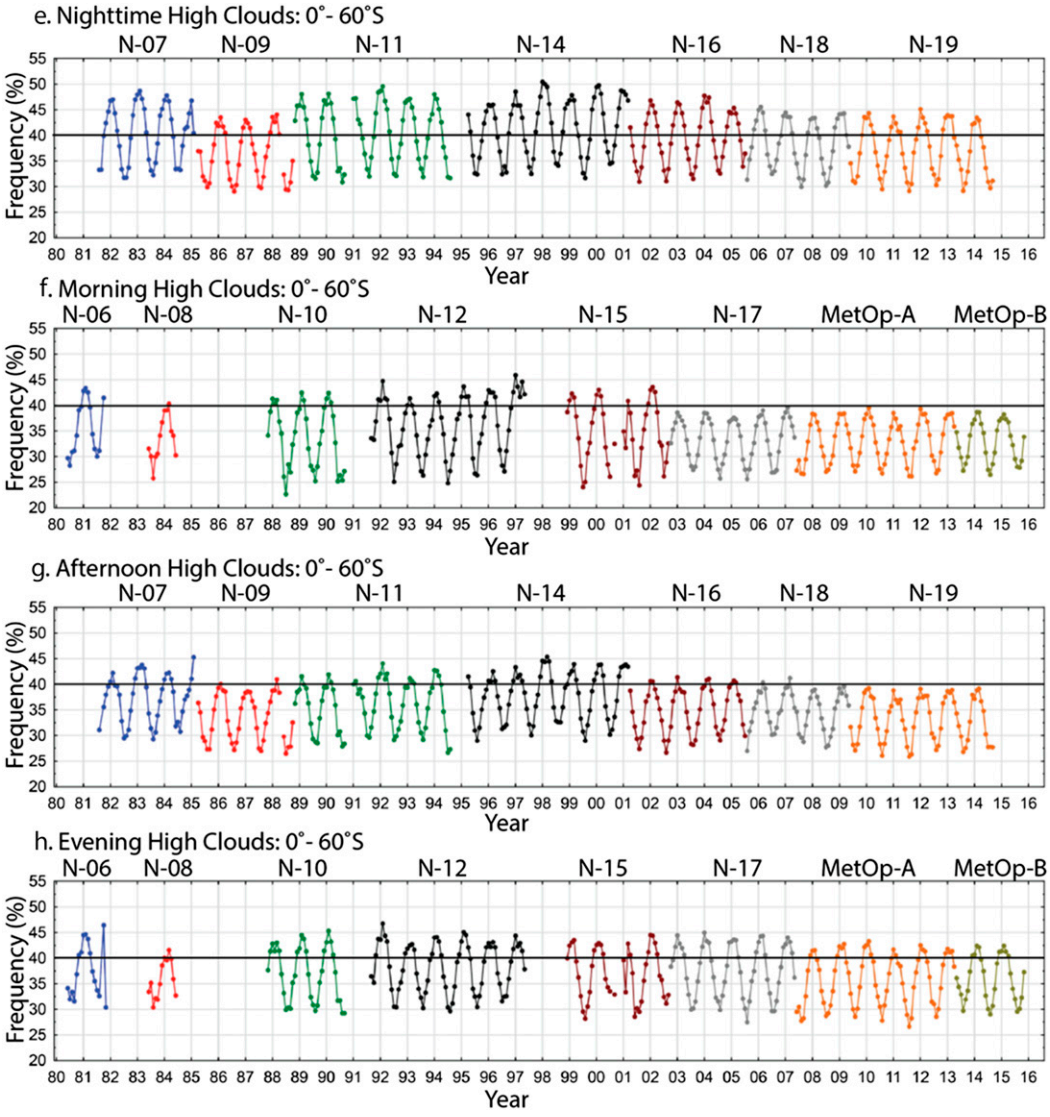

FIG. 5. (*Continued*)

high-cloud coverage is again evident. Fewer clouds (1%–3%) are found in the evening than at night.

In addition to orbit drift and sensor-to-sensor calibration issues, determination of cloud-detection trends is complicated by the change in HIRS FOV size. In both Figs. 2a–c and 2d–f, there is the indication that the 10-km HIRS FOV (on *NOAA-18*, *NOAA-19*, *MetOp-A*, and *MetOp-B*) sees fewer clouds than does the 20-km HIRS FOV (up to 5% depending on time of day and latitudinal region).

Further inspection of the AVHRR cloud mask collocated within the HIRS FOVs for one day (8 July 2007) revealed clear skies for 25.1% of the *NOAA-17* 20-km FOVs as compared with 27.3% of the *MetOp-A* 10-km FOVs. In the subsequent cloud processing, *MetOp-A* HIRS found 5% more opaque clouds, and correspondingly *NOAA-17* HIRS found 5% more thin and thick clouds. The high-, mid-, and low-cloud distributions were within 1% for each category.

The 1980–2015 mean HIRS high-cloud detection at night for January, April, July, and October is found in Fig. 3. The seasonal movement of the intertropical convergence zone is readily apparent, as is the October onset of high clouds over South America and Africa that last into April. Subtropical subsidence regions are also identified by the dearth of high clouds detected.

d. Zonal high clouds by morning, afternoon, evening, and night

Figure 4 shows the latitudinal average of the night, morning, afternoon, and evening high-cloud detection

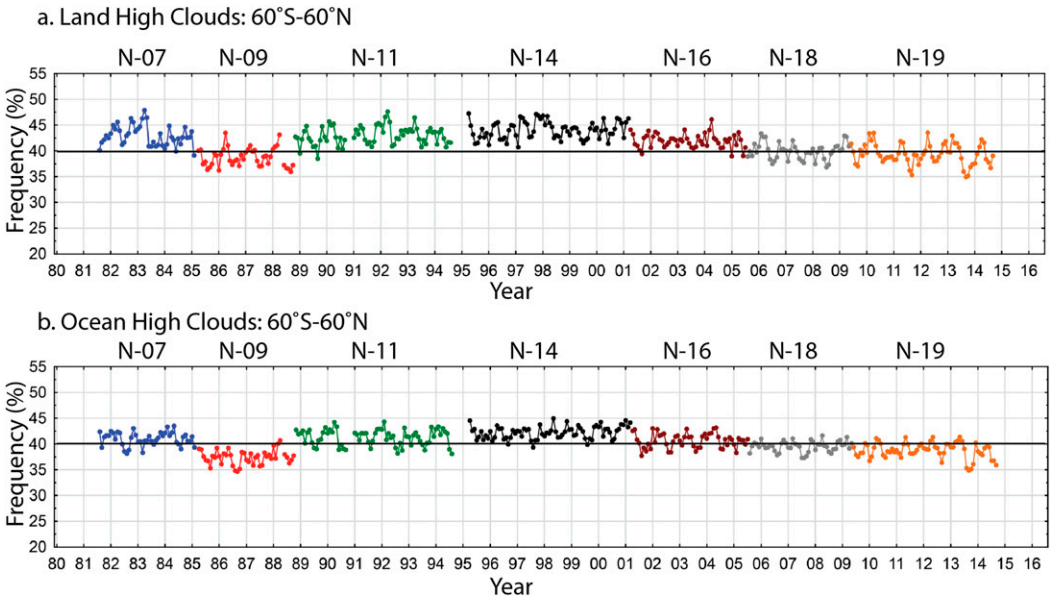

FIG. 6. Percentage of HIRS nighttime observations that contained high clouds over (a) land and (b) ocean from 60°S to 60°N from 1981 to 2014.

for the Northern Hemisphere winters (DJF; Figs. 4a,b) and summers (JJA; Figs. 4c,d) from 1980 to 2015. The DJF 50%–60% peak occurrence of tropical high clouds in the HIRS observations increases to 60%–70% during JJA; the DJF peak at 10°S shifts to 10°N in JJA. High-cloud detection is greater in the evening and night than in the morning and afternoon except in the southern midlatitudes for DJF, when morning is greater than evening. The midlatitude peaks in high-cloud detection between 35% and 40% stay at or near 45°S summer and winter in the Southern Hemisphere but shift from about 35°N in winter to near 50°N during summer in the Northern Hemisphere. The evening and nighttime maximum in the tropics is likely due to diurnal maximum of convection over ocean at evening/night and convection over land in the afternoon that results in more cirrus outflow in the evening and at night.

e. *Hemispheric high-cloud comparison*

The hemispheric balance of monthly high-cloud detection from 1980 to 2015 is explored in Fig. 5. The Northern Hemisphere (Figs. 5a–d) is found to be out of phase with the Southern Hemisphere (Figs. 5e–h). Further, the amplitude of seasonal changes is greater in the Southern Hemisphere than in the Northern Hemisphere. Orbital drift is particularly apparent in the Northern Hemisphere afternoon data for *NOAA-11* and *NOAA-14* (percentage of high clouds increases with time as observations move to later local times). It is less apparent in the Southern Hemisphere, presumably because of fewer land-based convective high clouds associated with solar heating.

f. *Land vs ocean high-cloud comparison*

Separation of the high-cloud detection at night over land from that over ocean is presented in Fig. 6. More high clouds (2%–3%) are found over land than over ocean; the persistence at night of high thin clouds after daytime convection has been noted in earlier work (Menzel et al. 1990). The seasonal cycles for high clouds over land are in phase with those over ocean; both are in phase with the Southern Hemisphere detection of high clouds. Sensor-to-sensor differences are evident. *NOAA-9* sees fewer high clouds. There is a modest drop off in high-cloud detection with the transition to the 10-km FOV in *NOAA-18* and *NOAA-19*. High-cloud detection over ocean remains constant near 40% within the operational lifetime for each individual sensor; overall there is no discernable trend in the 35 years that are presented here.

5. Summary and conclusions

Recalibration of the HIRS sensors and introduction of the AVHRR characterization of the HIRS subpixel cloud cover have assisted this reprocessing to produce a cloud dataset with sensor-to-sensor differences that are mitigated but not eliminated. Remaining possible causes for the sensor-to-sensor cloud-property discontinuities include bad data in the HIRS IR windows (not recalibrated to date) or cloud-mask issues in the AVHRR PATMOS-x data; these will be studied in the next

reprocessing. Limiting the cloud dataset to the operational HIRS data has reduced but not eliminated the larger effects of orbital drift. Division of the dataset into four time periods within the day has enabled some diurnal distinctions. A few conclusions from the HIRS reprocessing of cloud properties using the MODIS CO_2-slicing algorithm follow.

- This HIRS reprocessed dataset presents a cloud record from 1980 onward.
- Cloud-detection trends are affected by orbital drift.
- Evening and nighttime high-cloud-detection frequency is usually greater than that in morning and afternoon.
- Observations with 10-km FOV (HIRS/4) see fewer high clouds than those with 20-km FOV (HIRS/3 and HIRS/2).
- Clouds are found in ~76.5% of HIRS observations over 60°N–60°S; high clouds are found in ~36.1% of the observations.
- Northern Hemisphere (NH) seasonal high-cloud detection is exactly out of phase with Southern Hemisphere (SH) high-cloud detection; the seasonal fluctuation is greater in the SH than in the NH.
- The 60°N–60°S high-cloud-detection trends are the sum of the interference between the NH and SH (Stephens et al. (2015) allude to such a hemispheric balance). Because the SH seasonal fluctuations dominate those of the NH, the global high-cloud minima and maxima are ''in sync'' with those of the SH.
- Although there may be regional trends, the 60°N–60°S high-cloud detection in these HIRS observations shows no discernable trend.

The reprocessed HIRS cloud data record with a short descriptive ''README'' file is, at the time of writing, available online (ftp.ssec.wisc.edu/pub/CIMSS_HIRS_monthly_mean_cloud_products/rf52).

Continuation of the AVHRR/HIRS cloud detection will be possible with AVHRR/IASI on MetOp and Visible Infrared Radiometer Suite/Cross-Track Infrared Sounder (VIIRS/CrIS) on the Suomi National Polar-Orbiting Partnership (NPP) and the Joint Polar Satellite System (JPSS). The high-spectral-resolution CrIS and IASI measurements can be averaged over the HIRS SRF to create HIRS-like measurements. The AVHRR cloud mask approach can be used with AVHRR and VIIRS to characterize the IASI and CrIS subpixel cloud cover. Creation of a 50+-yr HIRS-like cloud record will offer more opportunity to investigate global and hemispheric trends in cloud cover.

Acknowledgments. The authors gratefully acknowledge the support by NOAA and NASA that permitted us to take this HIRS cloud retrieval effort from a research-level project to a level that is closer to being ready for operational use (NOAA Contract NA15NES4320001 and NASA Contract NNG15HZ38C). In addition, we thank our colleagues at the National Centers for Environmental Information (NCEI) for establishing the dataset for broader user access. The PATMOS-x cloud-mask data were graciously provided by Dr. Andy Heidinger.

REFERENCES

Aoki, T., 1985: A method for matching the HIRS/2 and AVHRR pictures of TIROS-N satellites. *Tech. Proc. Second Int. TOVS Study Conf.*, Igls, Austria, Cooperative Institute for Meteorological Satellite Studies, 349–367.

Baum, B. A., B. A. Wielicki, P. Minnis, and L. Parker, 1992: Cloud-property retrieval using merged HIRS and AVHRR data. *J. Appl. Meteor.*, **31**, 351–369, doi:10.1175/1520-0450(1992)031<0351:CPRUMH>2.0.CO;2.

——, W. P. Menzel, R. A. Frey, D. C. Tobin, R. E. Holz, S. A. Ackerman, A. K. Heidinger, and P. Yang, 2012: MODIS cloud-top property refinements for collection 6. *J. Appl. Meteor. Climatol.*, **51**, 1145–1163, doi:10.1175/JAMC-D-11-0203.1.

Cao, C., M. Goldberg, and L. Wang, 2009: Spectral bias estimation of historical HIRS using IASI observations for improved fundamental climate data records. *J. Atmos. Oceanic Technol.*, **26**, 1378–1387, doi:10.1175/2009JTECHA1235.1.

Chen, R., and C. Cao, 2012: Physical analysis and recalibration of MetOp HIRS using IASI for cloud studies. *J. Geophys. Res.*, **117**, D03103, doi:10.1029/2011JD016427.

——, ——, and W. P. Menzel, 2013: Intersatellite calibration of NOAA HIRS CO_2 channels for climate studies. *J. Geophys. Res.*, **118**, 5190–5203, doi:10.1002/jgrd.50447.

Foster, M. J., and A. Heidinger, 2013: PATMOS-x: Results from a diurnally corrected 30-yr satellite cloud climatology. *J. Climate*, **26**, 414–425, doi:10.1175/JCLI-D-11-00666.1.

Frey, R. A., S. A. Ackerman, and B. J. Soden, 1996: Climate parameters from satellite spectral measurements. Part 1: Collocated AVHRR and HIRS/2 observations of spectral greenhouse parameter. *J. Climate*, **9**, 327–344, doi:10.1175/1520-0442(1996)009<0327:CPFSSM>2.0.CO;2.

Hannon, S. E., L. L. Strow, and W. W. McMillan, 1996: Atmospheric infrared fast transmittance models: A comparison of two approaches. *Optical Spectroscopic Techniques and Instrumentation for Atmospheric and Space Research II*, P. B. Hays and J. Wang, Eds., International Society for Optical Engineering (SPIE Proceedings, Vol. 2830), 94–105, doi:10.1117/12.256106.

Heidinger, A. K., A. T. Evan, M. J. Foster, and A. Walther, 2012: A naive Bayesian cloud-detection scheme derived from *CALIPSO* and applied within PATMOS-x. *J. Appl. Meteor. Climatol.*, **51**, 1129–1144, doi:10.1175/JAMC-D-11-02.1.

——, M. J. Foster, A. Walther, and X. Zhao, 2014: The Pathfinder Atmospheres–Extended AVHRR climate dataset. *Bull. Amer. Meteor. Soc.*, **95**, 909–922, doi:10.1175/BAMS-D-12-00246.1.

——, ——, D. Botambekov, M. Hiley, A. Walther, and Y. Li, 2016: Using the NASA EOS A-Train to probe the performance of the NOAA PATMOS-x cloud fraction CDR. *Remote Sens.*, **8**, 511, doi:10.3390/rs8060511.

Kalnay, E., and Coauthors, 1996: The NCEP/NCAR 40-Year Reanalysis Project. *Bull. Amer. Meteor. Soc.*, **77**, 437–471, doi:10.1175/1520-0477(1996)077<0437:TNYRP>2.0.CO;2.

Kolat, U., 2010: Re-evaluation of HIRS detection of high clouds. M.S. thesis, Dept. of Atmospheric and Oceanic Sciences, University of Wisconsin–Madison, 47 pp.

——, W. P. Menzel, E. Olson, and R. Frey, 2013: Very high cloud detection in more than two decades of HIRS data. *J. Geophys. Res.*, **118**, 3278–3284, doi:10.1029/2012JD018496.

Menzel, W. P., T. J. Schmit, and D. P. Wylie, 1990: Cloud characteristics over central Amazonia during GTE/ABLE 2B derived from multispectral visible and infrared spin scan radiometer atmospheric sounder observations. *J. Geophys. Res.*, **95**, 17 039–17 042, doi:10.1029/JD095iD10p17039.

——, and Coauthors, 2008: MODIS global cloud-top pressure and amount estimation: Algorithm description and results. *J. Appl. Meteor. Climatol.*, **47**, 1175–1198, doi:10.1175/2007JAMC1705.1.

Nagle, F. W., and R. E. Holz, 2009: Computationally efficient methods of collocating satellite, aircraft, and ground observations. *J. Atmos. Oceanic Technol.*, **26**, 1585–1595, doi:10.1175/2008JTECHA1189.1.

Pavolonis, M. J., A. K. Heidinger, and T. Uttal, 2005: Daytime global cloud typing from AVHRR and VIIRS: Algorithm description, validation, and comparisons. *J. Appl. Meteor.*, **44**, 804–826, doi:10.1175/JAM2236.1.

Saha, S., and Coauthors, 2010: The NCEP Climate Forecast System Reanalysis. *Bull. Amer. Meteor. Soc.*, **91**, 1015–1057, doi:10.1175/2010BAMS3001.1.

Schmetz, J., S. A. Tjemkes, M. Gube, and L. van de Berg, 1997: Monitoring deep convection and convective overshooting with Meteosat. *Adv. Space Res.*, **19**, 433–441, doi:10.1016/S0273-1177(97)00051-3.

Shi, L., J. J. Bates, and C. Cao, 2008: Scene radiance–dependent intersatellite biases of HIRS longwave channels. *J. Atmos. Oceanic Technol.*, **25**, 2219–2229, doi:10.1175/2008JTECHA1058.1.

Smith, N., W. P. Menzel, E. Weisz, A. K. Heidinger, and B. A. Baum, 2013: A uniform space–time gridding algorithm for comparison of satellite data products: Characterization and sensitivity study. *J. Appl. Meteor. Climatol.*, **52**, 255–268, doi:10.1175/JAMC-D-12-031.1.

Stephens, G. L., D. O'Brien, P. J. Webster, P. Pilewski, S. Kato, and J.-L. Li, 2015: The albedo of Earth. *Rev. Geophys.*, **53**, 141–163, doi:10.1002/2014RG000449.

Strow, L. L., S. E. Hannon, S. De-Souza Machado, H. E. Motteler, and D. C. Tobin, 2006: Validation of the Atmospheric Infrared Sounder radiative transfer algorithm. *J. Geophys. Res.*, **111**, D09S06, doi:10.1029/2005JD006146.

Tobin, D. C., H. E. Revercomb, C. C. Moeller, and T. S. Pagano, 2006: Use of Atmospheric Infrared Sounder high-spectral resolution spectra to assess the calibration of Moderate Resolution Imaging Spectroradiometer on EOS Aqua. *J. Geophys. Res.*, **111**, D09S05, doi:10.1029/2005JD006095.

Wylie, D. P., and W. P. Menzel, 1999: Eight years of high cloud statistics using HIRS. *J. Climate*, **12**, 170–184, doi:10.1175/1520-0442-12.1.170.

——, D. L. Jackson, W. P. Menzel, and J. J. Bates, 2005: Trends in global cloud cover in two decades of HIRS observations. *J. Climate*, **18**, 3021–3031, doi:10.1175/JCLI3461.1.